

PCDCNet: A Surrogate Model for Air Quality Forecasting with Physical-Chemical Dynamics and Constraints

Shuo Wang
shuowang.ai@gmail.com
School of Systems Science
Beijing Normal University
Beijing, China
D-ITET, ETH Zurich
Zurich, Switzerland

Yun Cheng
yun.cheng@sdsc.ethz.ch
Swiss Data Science Center
ETH Zurich
Zurich, Switzerland

Qingye Meng
hilbertmeng@gmail.com
ColorfulClouds
Technology Co.,Ltd.
Beijing, China

Olga Saukh
saukh@tugraz.at
Graz University of Technology
Graz, Austria
Complexity Science Hub
Vienna, Austria

Jiang Zhang
zhangjiang@bnu.edu.cn
School of Systems Science
Beijing Normal University
Beijing, China

Jingfang Fan*
jingfang@bnu.edu.cn
School of Systems Science / Institute
of Nonequilibrium Systems
Beijing Normal University
Beijing, China
Potsdam Institute for Climate Impact
Research
Potsdam, Germany

Yuanting Zhang
zhangyuanting@caiyunapp.com
ColorfulClouds
Technology Co.,Ltd.
Beijing, China

Xingyuan Yuan
yuan@caiyunapp.com
ColorfulClouds
Technology Co.,Ltd.
Beijing, China

Lothar Thiele
thiele@ethz.ch
D-ITET, ETH Zurich
Zurich, Switzerland

Abstract

Air quality forecasting (AQF) is critical for public health and environmental management, yet remains challenging due to the complex interplay of emissions, meteorology, and chemical transformations. Traditional numerical models, such as CMAQ and WRF-Chem, provide physically grounded simulations but are computationally expensive and rely on uncertain emission inventories. Deep learning models, while computationally efficient, often struggle with generalization due to their lack of physical constraints. To bridge this gap, we propose **PCDCNet**, a **surrogate model** that integrates numerical modeling principles with deep learning. PCDCNet explicitly incorporates emissions, meteorological influences, and domain-informed constraints to model pollutant formation, transport, and dissipation. By combining *graph-based spatial transport modeling*, *recurrent structures for temporal accumulation*, and *representation enhancement for local interactions*, PCDCNet achieves

state-of-the-art (SOTA) performance in **72-hour station-level** PM_{2.5} and O₃ forecasting while significantly reducing computational costs. Furthermore, our model is deployed in an online platform, providing free, real-time air quality forecasts, demonstrating its scalability and societal impact. By aligning deep learning with **physical consistency**, PCDCNet offers a practical and interpretable solution for AQF, enabling informed decision-making for both personal and regulatory applications.

CCS Concepts

• **Computing methodologies** → Neural networks; • **Applied computing** → Physics; *Environmental sciences*.

Keywords

Air quality forecasting, physical-chemical dynamics, PINNs, meteorology, emissions, deep learning, graph neural networks, surrogate modeling, photochemical reactions, real-time forecasting.

*Corresponding author.

Permission to make digital or hard copies of all or part of this work for personal or classroom use is granted without fee provided that copies are not made or distributed for profit or commercial advantage and that copies bear this notice and the full citation on the first page. Copyrights for components of this work owned by others than the author(s) must be honored. Abstracting with credit is permitted. To copy otherwise, or republish, to post on servers or to redistribute to lists, requires prior specific permission and/or a fee. Request permissions from permissions@acm.org.
Conference acronym 'XX, Woodstock, NY

© 2018 Copyright held by the owner/author(s). Publication rights licensed to ACM.
ACM ISBN 978-1-4503-XXXX-X/2018/06
<https://doi.org/XXXXXXX.XXXXXXX>

ACM Reference Format:

Shuo Wang, Yun Cheng, Qingye Meng, Olga Saukh, Jiang Zhang, Jingfang Fan, Yuanting Zhang, Xingyuan Yuan, and Lothar Thiele. 2018. PCDCNet: A Surrogate Model for Air Quality Forecasting with Physical-Chemical Dynamics and Constraints. In *Proceedings of Make sure to enter the correct conference title from your rights confirmation email (Conference acronym 'XX)*. ACM, New York, NY, USA, 18 pages. <https://doi.org/XXXXXXX.XXXXXXX>

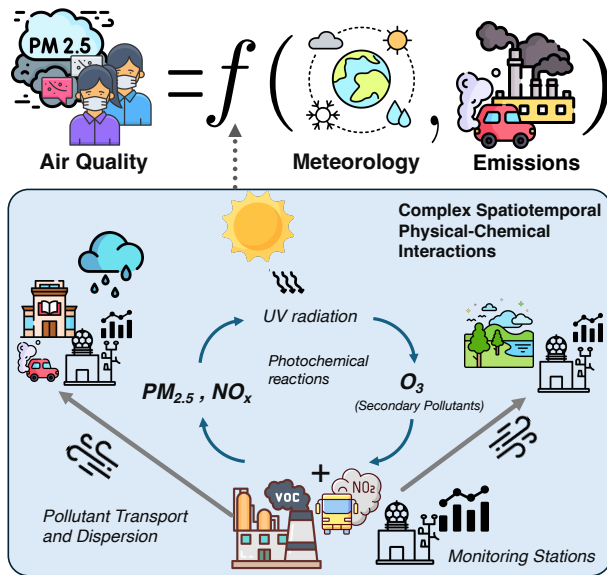


Figure 1: Air quality ($PM_{2.5}$ and O_3) is shaped by complex interactions between meteorology (e.g., UV radiation, wind) and emissions (e.g., NO_x , VOC). Capturing these spatiotemporal dynamics, including pollutant transport and secondary formation, requires integrating emissions data with meteorology, which poses significant modeling challenges.

1 Introduction

Air pollution remains a pressing global challenge, disproportionately affecting developing nations such as China, India, Pakistan, and Bangladesh [1, 5, 47]. Over the years, China has implemented rigorous measures to improve air quality, achieving significant reductions in $PM_{2.5}$ concentrations [18]. However, substantial gaps persist compared to the air quality standards of developed countries [48]. Furthermore, the reduction in $PM_{2.5}$ levels has inadvertently heightened the prominence of O_3 pollution [13, 33], exposing the intricate and nonlinear interactions between these pollutants and emphasizing the need for coordinated air pollution management strategies [7, 27].

In developed nations, while routine air quality levels are relatively better, catastrophic events like wildfires in Australia, the United States, and Canada have triggered severe pollution episodes, endangering public health [6, 8, 39]. These scenarios underscore the necessity of real-time, high-precision air quality forecasting (AQF) systems that can provide reliable site-specific predictions up to three days in advance. Such systems can serve as critical tools for personal protection, travel planning, and government interventions aimed at regulating industrial emissions, ultimately contributing to public health and environmental sustainability.

Air quality forecasting, particularly for key pollutants like $PM_{2.5}$ and O_3 , is inherently challenging due to the complex interplay of emissions, meteorology, and secondary chemical reactions [41, 43, 46]. As illustrated in Figure 1, pollutant concentrations are influenced by long-range spatiotemporal dependencies, where pollutants can travel vast distances under the influence of wind and

atmospheric dynamics [11, 12]. This results in local air quality being shaped not only by nearby emissions but also by regional and even global factors. Compounding this complexity, spatially proximate regions can exhibit starkly different pollution patterns due to variations in emission sources and industrial structures [18, 29, 50]. Moreover, many pollutants, such as O_3 , undergo complex chemical transformations, being formed as secondary pollutants through photochemical reactions involving NO_x and VOC under sunlight [30, 36]. These challenges necessitate the development of advanced models capable of integrating emissions and meteorology, capturing long-range dependencies, and modeling pollutant interactions.

Traditional numerical models like CMAQ (Community Multi-scale Air Quality model) [26, 34]¹ and WRF-Chem [40]² have long been the cornerstone of AQF [17]. These models solve partial differential equations (PDEs) to simulate the physical and chemical processes underlying pollutant formation, transport, and transformation. While these approaches provide interpretable insights, they are computationally expensive and unsuitable for real-time forecasting.

Moreover, their accuracy heavily depends on precisely estimated initial conditions, which are often difficult to obtain in practice [21, 37]. This reliance introduces significant uncertainty, especially in dynamic scenarios such as sudden pollution events. Additionally, these models are typically used retrospectively and lack native integration of real-time observational data [26], further limiting their adaptability to rapidly changing environmental conditions.

The advent of AI-based Earth system models, such as Pangu-Weather [3], GraphCast [25], and Aurora [4], have introduced a paradigm shift in geosciences, leveraging the strong pattern recognition capabilities of AI to efficiently model complex atmospheric phenomena. However, these models primarily focus on meteorological forecasting and often neglect the intricacies of air quality data. They typically operate on grid-based datasets like ERA5 reanalysis, which lack the spatial granularity and station-level variability of air quality monitoring systems.

Recently proposed transformer-based models, such as iTransformer [31] and TimeXer [45], have demonstrated remarkable advances on long-term time-series forecasting tasks. Yet, their generalized architectures are not specifically tailored for AQF. These models often fail to meet the high accuracy demands of AQF because they focus on learning generic temporal patterns rather than domain-specific dynamics like pollutant transport, interactions, and secondary formation. Existing AQF methods, on the other hand, either exclude critical variables like emissions data [44] or fail to adequately capture physical and chemical mechanisms [19, 42], leading to limited generalizability and suboptimal performance.

To this end, we introduce **PCDCNet**, a **surrogate model for AQF** that bridges numerical simulations and deep learning. PCDCNet captures **physical-chemical dynamics** while maintaining computational efficiency, serving as a data-driven alternative to traditional models. Unlike black-box deep learning methods, it explicitly integrates emissions, meteorology, and domain-informed constraints, ensuring both accuracy and interpretability. The key contributions of this work are as follows:

¹<https://www.epa.gov/cmaq>

²<https://www2.aom.ucar.edu/wrf-chem>

- **We propose PCDCNet, a surrogate modeling framework for AQF that ensures physical consistency while aligning with CMAQ-like numerical simulations.** By integrating emissions, meteorology, and spatiotemporal dynamics within a structured input-output framework, PCDCNet enforces atmospheric constraints, enabling interpretable and robust predictions.
- **We develop a hybrid architecture incorporating physical and chemical dynamics into deep learning, ensuring consistency and generalization.** PCDCNet leverages GRU for temporal accumulation, graph-based spatial transport modeling, and representation learning for pollutant interactions, with domain-informed constraints enforcing alignment with physical laws.
- **We deploy PCDCNet as a real-time AQF service, offering free and accessible forecasts.** Integrated into an online platform³, it delivers 72-hour station-level predictions, providing actionable insights for health protection, travel planning, and policy decisions.

By introducing a **physically consistent and computationally efficient** surrogate modeling paradigm, PCDCNet bridges numerical simulations and deep learning, reinforcing the role of domain knowledge in AI-driven environmental modeling.

2 Preliminaries

This section presents the datasets, research regions, spatial graph construction, and problem definition for AQF. Additionally, we compare input-output paradigms across numerical models, deep learning methods, and our approach.

2.1 Datasets and Research Regions

Our study utilizes air quality, meteorological, and emission datasets to tackle AQF challenges in two key regions of China: the **Beijing-Tianjin-Hebei and Surrounding Areas (BTHSA)**, spanning approximately **430,000 km²** and covering **2+26 cities** [32]⁴, and the **Yangtze River Delta (YRD)**, encompassing around **270,000 km²**. These regions exhibit diverse pollution characteristics, meteorological variations, and emission patterns, providing a comprehensive testbed for evaluating AQF models, as depicted in Figure 6. Appendix A.3 summarizes the variables used in this study.

Air Quality Data. Hourly PM_{2.5} and O₃ concentrations from 355 monitoring stations across **BTHSA** and **YRD** (Figure 6) were sourced from CNEMC⁵. These datasets provide high spatial and temporal resolution, enabling detailed analysis of pollution dynamics in both urban and rural areas.

Meteorological Data. Key meteorological variables, including wind components (u100, v100), temperature (t2m), precipitation (tp), surface pressure (sp), and others, were sourced from the ERA5 reanalysis dataset⁶. For deployment, we utilized GFS forecast data⁷, which provides hourly predictions updated four times daily.

Emission Data. Regional emissions of NO_x, VOC, SO₂, NH₃, and PM_{2.5} were obtained from the Multi-resolution Emission Inventory for China (MEIC) [18, 29]⁸. These monthly inventories, while statistical estimates, capture general emission trends and were down-scaled to an hourly resolution using the methodology in [16] to align with air quality and meteorological data.

Graph Construction. A spatial adjacency graph was constructed by connecting monitoring stations within a 200km geodesic threshold, as shown in Figure 6, following [35, 42]. This graph models pollutant transport pathways and underpins the GNN-based components of our framework.

2.2 Problem Statement, Inputs and Outputs

The goal of AQF is to predict future pollutant concentrations using historical data and forecasted meteorology and emissions. As shown in Figure 7, given historical pollutant concentrations $\mathbf{X}^{-T'+1:0}$, meteorological variables $\mathbf{P}^{-T'+1:0}$, and emissions $\mathbf{Q}^{-T'+1:0}$, along with forecasted meteorology $\mathbf{P}^{1:T}$ and emissions $\mathbf{Q}^{1:T}$, the objective is to estimate $\hat{\mathbf{X}}^{1:T}$:

$$\hat{\mathbf{X}}^{1:T} = \mathcal{F}_{\Theta} \left(\mathbf{X}^{-T'+1:0}, \mathbf{P}^{-T'+1:T}, \mathbf{Q}^{-T'+1:T} \right), \quad (1)$$

where \mathcal{F}_{Θ} models spatiotemporal dependencies, pollutant transport, and secondary pollutant formation.

3 Methodology

This section introduces PCDCNet, a surrogate model that integrates emissions, meteorology, and physical-chemical constraints for efficient and interpretable AQF. By embedding atmospheric processes such as **advection, diffusion, deposition, and secondary formation**, PCDCNet bridges the gap between **numerical simulations (e.g., CMAQ)** and **AI-based methods**.

3.1 Model Overview

Traditional chemical transport models (CTMs), such as CMAQ, describe pollutant evolution through a set of partial differential equations (PDEs) that account for various atmospheric processes, including advection, diffusion, deposition, emissions, and chemical reactions [20, 38]. The general form of pollutant concentration C at time t is governed by:

$$\frac{\partial C_i}{\partial t} = -\mathbf{u} \cdot \nabla C_i + \nabla \cdot (k \nabla C_i) + R + D + S, \quad (2)$$

where \mathbf{u} represents wind vectors (advection), k is the diffusion coefficient, R accounts for chemical reactions, and D , S denote deposition and source terms, respectively.

Traditional methods face significant limitations, including their dependence on preprocessed meteorological inputs (e.g., WRF), which introduces uncertainties and restricts the use of direct NWP products like GFS and ECMWF, as well as reliance on initial condition fields with high uncertainty impacting prediction accuracy. Additionally, limited integration with station-level data reduces adaptability to local pollution dynamics, while high computational costs hinder their feasibility for real-time applications.

³PCDCNet-powered AQF: <https://caiyunapp.com/map>

⁴https://www.mee.gov.cn/gkml/sthjbgw/qt/201701/t20170124_395229.htm

⁵<https://www.cnemc.cn/>

⁶<https://cds.climate.copernicus.eu/datasets/reanalysis-era5-single-levels>

⁷<https://www.ncei.noaa.gov/products/weather-climate-models/global-forecast>

⁸<http://meicmodel.org.cn/>

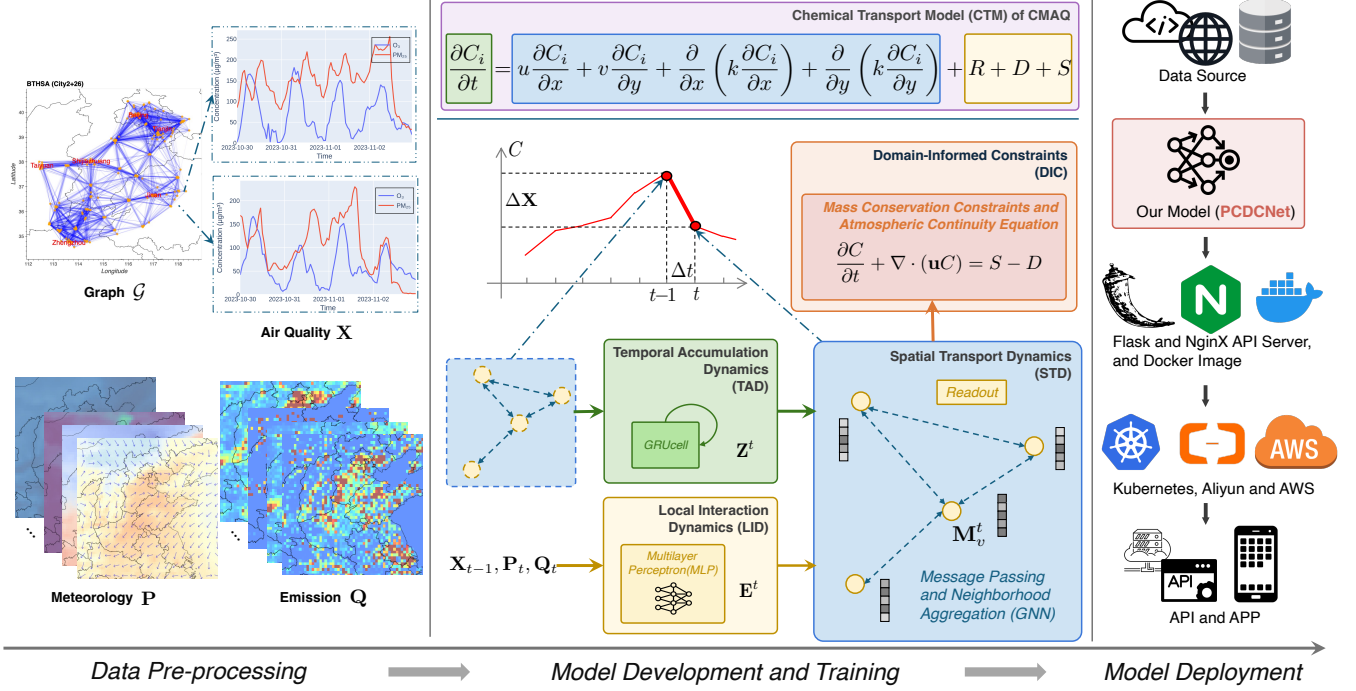


Figure 2: The framework of PCDCNet for air quality forecasting (AQF), comprising three stages: Data Pre-processing (graph construction and integration of X, P, Q), Model Development (modules for temporal, spatial, and local dynamics with domain-informed constraints), and Model Deployment (real-time predictions via cloud-based Dockerized APIs).

To overcome traditional limitations, we introduce **PCDCNet**, a deep learning-based surrogate model for air quality forecasting (AQF) that integrates the physical and chemical principles of CTMs with data-driven learning. As shown in Figure 2, PCDCNet incorporates emissions, meteorology, and pollutant dynamics within a structured spatiotemporal framework, consisting of three core modules:

- **Local Interaction Dynamics (LID)**: Models localized pollutant interactions (e.g., secondary formation) using emissions, meteorology, and concentrations via an MLP.
- **Spatial Transport Dynamics (STD)**: Captures pollutant advection and dispersion through graph-based message passing for long-range dependencies.
- **Temporal Accumulation Dynamics (TAD)**: Learns temporal patterns and pollutant persistence using a GRU for historical trends and decay dynamics.

Pseudo-code Implementation Algorithm 1 provides the pseudo-code for the training and inference process of PCDCNet, highlighting the interactions among those modules. The **Embed** step maps input data into the hidden space, while the **Readout** step translates the hidden space representation into the predicted outputs.

3.2 Core Modules

PCDCNet integrates three modules—**LID**, **STD**, and **TAD**—to model local interactions, pollutant transport, and temporal accumulation, ensuring a **physically consistent and data-driven** framework, as illustrated in Figure 2.

3.2.1 Local Interaction Dynamics (LID). The LID module captures pollutant interactions by embedding **meteorology (P)**, **emissions (Q)**, and **air pollutant concentrations (X)** into a latent space representation. This process consists of two key stages:

First, the initial hidden state H^t is obtained through an embedding step:

$$H^t = \text{Linear}([\hat{X}^{t-1}, P^t, Q^t]), \quad (3)$$

where \hat{X}^{t-1} is the estimated pollutant concentration from the previous step, while P^t and Q^t represent the meteorological and emissions variables at time t . The Linear layer projects these inputs into the hidden space.

Next, a representation enhancement step refines H^t using a multi-layer perceptron (MLP) with normalization:

$$E^t = \text{MLP}(\text{RMSNorm}(H^t)), \quad (4)$$

where the MLP applies nonlinear transformations, incorporating **Linear layers**, **RMSNorm** [49]⁹, **SiLU**¹⁰, and **Dropout** to improve feature expressiveness. This step enhances pollutant interactions, accounting for complex photochemical reactions, emissions-driven variations, and meteorological influences.

⁹<https://pytorch.org/docs/stable/generated/torch.nn.modules.normalization.RMSNorm.html>

¹⁰<https://pytorch.org/docs/stable/generated/torch.nn.SiLU.html>

Algorithm 1 Training and inference procedure of PCDCNet.

Require: Training dataset $\mathcal{D} = \{D_n\}_{n=1}^N$, initialized parameters Θ , learning rate α

Ensure: Optimized Θ (training), sequence $\{\hat{X}\}_{t=1}^T$ (inference)

```

1: for each sample  $D_k = (X, P, Q) \in \mathcal{D}$  do
2:   Initialize  $Z^{-T'+1} = \mathbf{0}$ 
3:   for  $t = -T' + 2$  to  $T$  do  $\triangleright t_0$  marks the last observed AQI
     in the sample; time steps correspond to its sliding window. In
     online deployment,  $t_0$  is the current time.
4:      $H^t = \begin{cases} \text{Linear}([X^{t-1}, P^t, Q^t]), & \text{if } t < 1 \\ \text{Linear}([\hat{X}^{t-1}, P^t, Q^t]), & \text{otherwise} \end{cases} \triangleright$ 
     Embedding: Use ground truth  $X$  for historical phase, previous
     estimate  $\hat{X}$  for prediction.
5:      $E^t = \text{MLP}(H^t); \quad H^t \leftarrow E^t \quad \triangleright \text{LID}$ 
6:      $M^t = \text{MessagePassing}(H^t, \mathcal{G}); \quad H^t \leftarrow M^t \quad \triangleright \text{STD}$ 
7:      $Z^t = \text{GRUcell}(H^t, Z^{t-1}); \quad H^t \leftarrow Z^t \quad \triangleright \text{TAD}$ 
8:      $\Delta \hat{X}^t = \text{Linear}(H^t); \quad \hat{X}^t = \hat{X}^{t-1} + \Delta \hat{X}^t \quad \triangleright \text{Readout}$ 
9:     if  $t \geq 1$  then  $\triangleright$  Prediction phase
10:      Store  $\hat{X}^t; \quad \nabla \hat{X}_M^t = \text{Linear}(M^t) \quad \triangleright \text{STD Readout}$ 
11:       $\mathcal{L}_{\text{DIC}} \leftarrow \text{DIC}(\nabla \hat{X}_M^{t-1}, \nabla \hat{X}_M^t) \quad \triangleright \text{DIC}$ 
12:    end if
13:  end for
14: end for
15:  $\mathcal{L} \leftarrow \mathcal{L}_{\text{L1}} + \lambda \mathcal{L}_{\text{DIC}}; \quad \Theta \leftarrow \Theta - \alpha \frac{\partial \mathcal{L}}{\partial \Theta} \quad \triangleright \text{Loss update}$ 
16: return  $\Theta$  (training) or  $\{\hat{X}\}_{t=1}^T$  (inference)
```

3.2.2 Spatial Transport Dynamics (STD). The STD module models **pollutant transport and dispersion**, capturing advection and diffusion effects across a spatial graph $\mathcal{G} = (\mathcal{V}, \mathcal{E})$. Here, each node $v \in \mathcal{V}$ represents a monitoring station, while edges \mathcal{E} define spatial connections based on a predefined geodesic distance threshold (e.g., 200 km).

To propagate pollutant states across space, we employ a **graph convolutional operation** [24] that aggregates information from neighboring nodes while ensuring numerical stability through a Laplacian-based normalization:

$$M^t = \text{Linear}(\tilde{L}H^t) = \text{Linear}((I - D^{-1/2}AD^{-1/2})H^t), \quad (5)$$

where:

- A is the adjacency matrix, encoding the connectivity between stations.
- D is the diagonal degree matrix, where $D_{vv} = \sum_{v' \in \mathcal{N}(v)} A_{vv'}$.
- \tilde{L} is the **normalized graph Laplacian**, which ensures balanced information propagation across nodes with varying connectivity.

This formulation allows the model to **capture pollutant dispersion as a second-order process** [24, 28, 38], effectively representing spatial diffusion and advection mechanisms in air quality dynamics. The Laplacian normalization further stabilizes computation across nodes with different degrees, making pollutant transport modeling both scalable and physically meaningful.

To enforce **mass conservation** [38], we introduce a **domain-informed constraint (DIC)** that ensures the net transported pollutant mass remains balanced across all nodes at each time step:

$$\sum_{v \in \mathcal{V}} \nabla \hat{X}_M^t = 0, \quad (6)$$

where $\nabla \hat{X}_M^t$ represents the predicted pollutant transport gradient. This loss encourages the model to **maintain pollutant mass balance**, preventing unphysical accumulation or dissipation.

3.2.3 Temporal Accumulation Dynamics (TAD). The TAD module captures **long-term pollutant accumulation and decay** by modeling sequential dependencies using a gated recurrent unit (GRU). Given the outputs from LID and STD, the TAD module updates the hidden state as:

$$Z^t = \text{GRUcell}(H^t, Z^{t-1}). \quad (7)$$

This recurrent structure enables PCDCNet to track pollution trends over time, accounting for **pollutant persistence, decay, and meteorology-driven changes**. Unlike transformer-based models that treat time steps as independent tokens, GRU explicitly accumulates past data, improving robustness for long-term forecasting.

3.3 Prediction Framework and Loss

As shown in Algorithm 1, PCDCNet employs an iterative prediction strategy to ensure smooth and stable pollutant forecasts. At each time step t , the model first estimates the rate of change in pollutant concentration:

$$\Delta \hat{X}^t = \text{Linear}(H^t). \quad (8)$$

The updated pollutant concentration is then obtained using a **residual formulation**, refining predictions through step-wise accumulation:

$$\hat{X}^t = \hat{X}^{t-1} + \Delta \hat{X}^t. \quad (9)$$

This formulation enables the model to iteratively correct its predictions, preserving physical consistency while mitigating abrupt fluctuations. By modeling pollutant evolution as a sequential adjustment process, PCDCNet achieves stable and reliable long-term forecasts.

3.3.1 Loss Functions and Mass Conservation Constraints. To ensure accurate predictions while maintaining consistency with atmospheric processes, PCDCNet optimizes the following objective:

$$\mathcal{L} = \mathcal{L}_{\text{L1}} + \lambda \mathcal{L}_{\text{DIC}}. \quad (10)$$

where:

- \mathcal{L}_{L1} is the **prediction loss**, minimizing the absolute error between predicted and observed pollutant concentrations:

$$\mathcal{L}_{\text{L1}} = \frac{1}{NT} \sum_{n=1}^N \sum_{t=1}^T \|\hat{X}_n^t - X_n^t\|_1. \quad (11)$$

- \mathcal{L}_{DIC} enforces **mass conservation** constraints on the STD module, ensuring physically consistent transport of pollutants.

3.3.2 Enforcing Mass Conservation in STD. In atmospheric sciences, pollutant transport follows the **continuity equation** [22], ensuring pollutants are transported without artificial mass gain or loss. To align with this principle, we explicitly extract the **spatial transport contribution** from the STD module at each prediction step:

$$\nabla \hat{\mathbf{X}}_{\mathbf{M}}^t = \text{Linear}(\mathbf{M}_t). \quad (12)$$

This term explicitly represents the **modeled pollutant transport effect** from the STD module. To ensure mass balance across both space and time, PCDCNet applies a **domain-informed constraint (DIC)** that enforces continuity in pollutant transport:

$$\mathcal{L}_{\text{DIC}} = \sum_{t=1}^T \|\nabla \hat{\mathbf{X}}_{\mathbf{M}}^t - \nabla \hat{\mathbf{X}}_{\mathbf{M}}^{t-1}\|_2. \quad (13)$$

To further ensure that pollutant transport strictly follows physical principles, we impose two **mass conservation constraints**:

- **Spatial Mass Conservation** At each step, the total pollutant mass exchanged between connected nodes in the station graph (\mathcal{G}) must sum to zero, preserving balance and preventing artificial generation or dissipation of pollutants:

$$\sum_{v' \in \mathcal{N}(v)} \nabla \hat{\mathbf{X}}_{\mathbf{M}, v \rightarrow v'}^t = 0, \quad \forall v \in \mathcal{V}. \quad (14)$$

Here, $\nabla \hat{\mathbf{X}}_{\mathbf{M}, v \rightarrow v'}^t$ represents the pollutant flux from node v to its neighbor v' , directly extracted from STD. This ensures that pollutants transported away from a node must reappear in its neighboring nodes.

- **Temporal Mass Conservation** The total pollutant mass across all nodes should remain stable over time, preventing artificial sources or sinks:

$$\frac{d}{dt} \sum_{v \in \mathcal{V}} \nabla \hat{\mathbf{X}}_{\mathbf{M}, v}^t = 0. \quad (15)$$

3.3.3 DIC Loss Formulation. To integrate these constraints into training, we define the final domain-informed loss:

$$\mathcal{L}_{\text{DIC}} = \frac{1}{|\mathcal{V}|} \sum_v \left| \sum_{v' \in \mathcal{N}(v)} \nabla \hat{\mathbf{X}}_{\mathbf{M}, v \rightarrow v'}^t \right| + \frac{1}{T} \sum_t \left| \sum_v \frac{d \nabla \hat{\mathbf{X}}_{\mathbf{M}, v}^t}{dt} \right|. \quad (16)$$

3.3.4 Interplay Between STD and GRU in PCDCNet. While the STD module is explicitly constrained to enforce pollutant transport physics, **pollutant accumulation and secondary transformations** (e.g., chemical reactions, deposition effects) are handled by the GRU-based TAD. The GRU is responsible for learning time-dependent variations, including pollutant persistence, atmospheric reactions, and slow temporal drifts, while the STD ensures instantaneous pollutant transport follows physical constraints.

By constraining pollutant movement within STD and allowing GRU to model long-term temporal dynamics, PCDCNet achieves **physically grounded yet flexible pollutant forecasting**, ensuring improved generalization and interpretability.

3.4 Deployment Framework

The deployment pipeline for PCDCNet ensures real-time readiness, scalability, high availability, and concurrency, as illustrated in Figure 2. Preprocessed inputs, including historical air quality, meteorological forecasts (e.g., GFS), and emissions, are fed into PCDCNet, which outputs pollutant predictions via a Flask and NginX API framework. Containerized with Docker and orchestrated through Kubernetes, the system supports dynamic scaling across cloud platforms like AWS and Aliyun. To ensure high availability and concurrency, redundant deployments, load balancing, and asynchronous endpoints are employed, while meteorological updates, provided four times daily, align predictions with real-time needs.

4 Experiments

This section evaluates the effectiveness of PCDCNet for air quality forecasting (AQF) using real-world datasets. We detail the experimental setup, including dataset configuration, implementation details, and baseline comparisons, followed by a comprehensive analysis of results.

4.1 Experimental Setup

4.1.1 Dataset. To ensure robust evaluation, we construct a large-scale dataset spanning 2016–2023, incorporating air quality, meteorological, and emissions data. The dataset includes a total of **70,128 hours** of observations from **355 monitoring stations**. It comprises **2 air quality variables** (e.g., $\text{PM}_{2.5}$ and O_3), **6 emissions variables** (e.g., NO_x , VOC), and **8 meteorological variables** (e.g., temperature, wind components). The years 2016–2019 are used for training, 2020–2021 for validation and hyperparameter tuning, and 2022–2023 for testing. This split ensures fair evaluation of model generalization. A detailed summary of the dataset variables is provided in Appendix A.3.

4.1.2 Implementation Details. PCDCNet is implemented using PyTorch, with graph-based computations handled by PyTorch Geometric (PyG) [15]. Training is conducted on an Nvidia 4070S GPU, enabling efficient large-scale experiments. The model is optimized for deployment on CPUs, ensuring computational efficiency and cost-effectiveness.

The training process employs the Adam optimizer with an initial learning rate of 1×10^{-4} , a batch size of 32, and runs for 100 epochs. Early stopping is applied based on validation MAE to prevent overfitting, and a learning rate scheduler (ReduceLROnPlateau) is used for dynamic adjustment. To improve computational efficiency, mixed precision training with FP16 is enabled.

Evaluation Metrics. To quantitatively assess the forecasting accuracy of PCDCNet, we employ **Mean Absolute Error (MAE)** and **Root Mean Square Error (RMSE)**. MAE provides an interpretable measure of absolute prediction error, while RMSE penalizes larger deviations, making it more sensitive to extreme prediction errors. The definitions of these metrics are provided in Appendix A.7.

4.1.3 Baselines. We evaluate PCDCNet against three categories of baseline models, with Table 3 in Appendix A.6 summarizing their key modeling characteristics. Additionally, Figure 7 in Appendix A.5

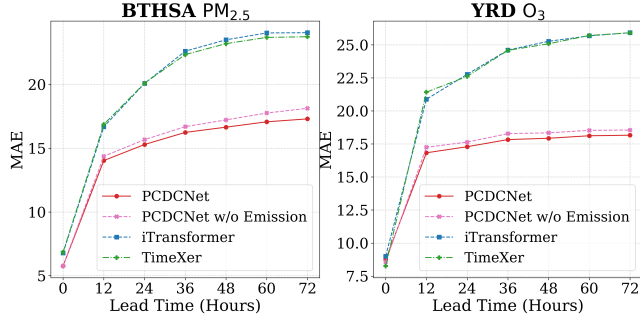


Figure 3: MAE trends for $\text{PM}_{2.5}$ in BTHSA and O_3 in YRD over a 72-hour prediction horizon.

illustrates their input-output frameworks based on their original designs.

- **Machine Learning Models:** These include **XGBoost** [10] and **LightGBM** [23], which directly fit air quality predictions to meteorological and emissions data using gradient boosting but lack temporal and spatial modeling.
- **General Time-Series Forecasting Models:** These include transformer-based architectures such as **iTransformer** [31]¹¹ and **TimeXer** [45]¹², which model historical air quality, meteorology, and emissions in the encoder but predict air quality directly in the decoder without incorporating forecasted meteorological data.
- **Air Quality Forecasting (AQF) Models:** These methods are specifically tailored for air pollution forecasting, integrating spatiotemporal and, in some cases, physical constraints. Notable examples include **GC-LSTM** [35], a hybrid model combining graph convolution (GCN) and LSTM for spatiotemporal prediction; **$\text{PM}_{2.5}$ -GNN** [44]¹³, a GNN-based model incorporating meteorological inputs but lacking explicit physical constraints; and **AirPhyNet** [19]¹⁴, a physics-informed neural ODE [9] model using historical air quality and wind to construct advection-diffusion kernels, without other meteorological or emissions inputs.

4.2 Performance Analysis

Table 1 compares PCDCNet with both traditional (e.g., XGBoost, LightGBM) and advanced (e.g., iTransformer, TimeXer) models on a 72-hour AQF task in the BTHSA and YRD regions. PCDCNet consistently achieves the lowest MAE across both pollutants and regions. Notably, it reduces the prediction error by **19.8%** for $\text{PM}_{2.5}$ and **18.4%** for O_3 compared to the next best method. This improvement is especially pronounced for long lead times of 72, underscoring the model’s robustness in scenarios where baseline methods often experience accumulating errors.

Figure 3 further illustrates these gains by showing the MAE trends for $\text{PM}_{2.5}$ in BTHSA and O_3 in YRD over the full 72-hour horizon. While competing approaches see their errors increase

sharply with extended lead times, PCDCNet maintains relatively stable performance, demonstrating its capacity to retain predictive accuracy even under longer forecasting windows.

CMAQ Input-Output Framework. These results strongly echo our argument from the Introduction that a surrogate model grounded in numerical modeling principles can offer both computational efficiency and physical consistency. By aligning the input-output structure of PCDCNet with how CMAQ (and similar systems) incorporate meteorological forecasts and emissions data, we capture the multi-scale dynamics underpinning air quality. This design choice yields a meaningful reduction in errors over purely time-series-based architectures, particularly for secondary pollutants like O_3 , which are sensitive to meteorological variations and photochemical reactions.

Error Reductions Through Emissions. Unlike general-purpose transformer models, PCDCNet explicitly integrates forecasted meteorology and emissions. This focus on domain-specific drivers yields error reductions of **9.8%** in $\text{PM}_{2.5}$ and **3.7%** in O_3 predictions over baselines lacking emissions data (Figure 15 in Appendix A.10). These improvements validate the need for pollutant-specific modeling strategies where meteorological conditions and emissions intricacies are paramount.

Long-Term Stability and Physical Consistency. Finally, the stable performance at extended lead times aligns with the emphasis on bridging physics-based insights with data-driven flexibility. By maintaining a structured framework that enforces mass conservation and accounts for transport processes, PCDCNet mitigates error propagation and delivers physically plausible forecasts over 72 hours. In doing so, it serves as a computationally efficient surrogate that remains interpretable and reliable—a critical requirement for real-time air quality management and decision-making.

4.3 Ablation Studies and Parameter Sensitivity

To evaluate the contributions of individual components and hyperparameter choices in PCDCNet, we conduct ablation studies and sensitivity analysis, as shown in Figure 5.

Ablation Studies. Ablation results demonstrate the importance of **LID**, **STD**, and **TAD**. Removing **LID** weakens the model’s ability to capture nonlinear interactions, while excluding **STD** impacts pollutant transport modeling. The largest performance drop occurs when **TAD** is omitted, underscoring its critical role in capturing temporal dependencies and propagating historical information.

Parameter Sensitivity. Sensitivity analysis shows that a hidden size of 32 achieves the best balance between model capacity and computational efficiency, outperforming smaller sizes prone to underfitting and larger sizes prone to overfitting. These results validate PCDCNet’s design and its ability to achieve robust air quality forecasting accuracy.

4.4 Physical Consistency and Generalization

Figure 4 illustrates the impact of the Domain-Informed Constraints (DIC) loss under varying strengths of the hyperparameter λ , where $\lambda = 0$ indicates the absence of DIC loss (only \mathcal{L}_{L1} is used), and $\lambda = 10$ applies stronger constraints.

¹¹<https://github.com/thuml/iTransformer>

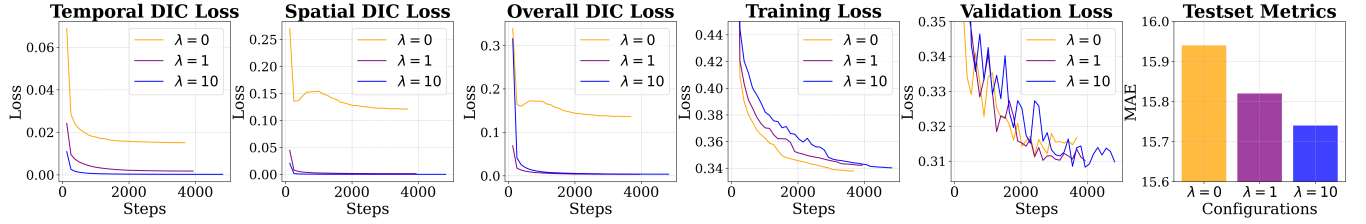
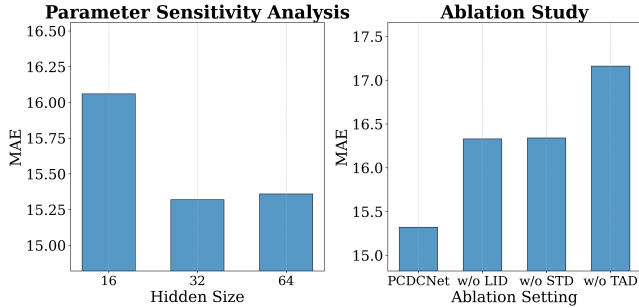
¹²<https://github.com/thuml/TimeXer>

¹³<https://github.com/shuowang-ai/PM2.5-GNN>

¹⁴<https://github.com/kethmih/AirPhyNet>

Table 1: Performance comparison of models on BTHSA and YRD data in a 72-hour forecasting task. The reported metrics are the average RMSE and MAE across all time steps compared with the ground truth.

Model (Publication)	BTHSA				YRD			
	RMSE ↓		MAE ↓		RMSE ↓		MAE ↓	
	PM _{2.5}	O ₃	PM _{2.5}	O ₃	PM _{2.5}	O ₃	PM _{2.5}	O ₃
XGBoost [10] (NeurIPS'16)	35.47	<u>27.53</u>	26.05	<u>20.68</u>	22.07	<u>27.71</u>	16.64	<u>20.99</u>
LightGBM [23] (NeurIPS'17)	35.48	27.97	26.07	21.05	22.06	28.07	16.74	21.33
GC-LSTM [35] (STOTEN'19)	32.95	35.12	23.09	26.82	18.77	34.65	13.57	26.31
PM _{2.5} -GNN [44] (SIGSPATIAL'20)	31.51	31.85	23.5	22.9	18.17	31.46	13.24	24.05
iTransformer [31] (ICLR'23)	<u>31.17</u>	29.9	20.72	22.58	17.92	30.53	<u>12.86</u>	23.28
AirPhyNet [19] (ICLR'24)	50.49	68.04	40.26	51.53	28.53	56.96	22.9	42.76
TimeXer [45] (NeurIPS'24)	31.51	30.07	<u>20.6</u>	22.87	<u>17.89</u>	30.47	<u>12.86</u>	23.28
PCDCNet (Ours)	24.13	22.45	15.46	16.73	15.55	23.03	10.97	17.27

**Figure 4: Analysis of Domain-Informed Constraints (DIC). Temporal and spatial DIC loss components confirm the necessity of separately modeling pollutant conservation across time and space. Stronger DIC constraints ($\lambda = 10$) improve test set performance while maintaining physical consistency.****Figure 5: Performance evaluation in BTHSA. (Left) Sensitivity analysis of hidden size (16, 32, 64) shows that 32 yields the lowest MAE, balancing complexity and generalization. (Right) Ablation study confirms performance drops when removing components, validating the model design.**

Impact on Test Set Performance. As λ increases, the test set MAE consistently decreases, demonstrating the effectiveness of the DIC loss in improving generalization. For $\lambda = 0$, the model lacks explicit constraints to enforce physical consistency, leading to suboptimal performance. Conversely, $\lambda = 10$ achieves the best results by strongly guiding the model toward domain-consistent behavior.

Implicit Mass Conservation in STD. Interestingly, even when $\lambda = 0$, the DIC loss curves (temporal, spatial, and overall) exhibit a

rapid initial decrease (Figure 4). This suggests that the STD module inherently learns to approximate mass conservation, despite the absence of constraints. However, without DIC loss, values stabilize at higher levels, indicating insufficient guidance for near-zero physical inconsistencies. When $\lambda > 0$, the DIC loss reduces significantly, validating the integration of domain knowledge into training.

Training and Validation Loss Dynamics. The training loss is lowest for $\lambda = 0$, as the absence of constraints allows the model to overfit. However, the validation loss shows the opposite trend: stronger DIC constraints ($\lambda = 10$) yield better generalization. This inversion underscores the role of DIC loss in improving robustness and alignment with physical laws.

Component-Wise Effectiveness. The temporal and spatial components of the DIC loss validate the necessity of separately modeling these two aspects of pollutant dynamics. Temporal DIC ensures consistency across time steps, while spatial DIC enforces pollutant conservation across neighboring nodes, together forming a comprehensive representation of atmospheric transport dynamics.

These results validate the design and integration of DIC loss into PCDCNet, showcasing its effectiveness in embedding domain knowledge and enhancing predictive accuracy and interpretability.

4.5 Online Deployment and Case Studies

Real-Time Deployment. PCDCNet has been deployed as a real-time AQF system¹⁵. Forecasted meteorological inputs, updated every six hours, are sourced from **GFS**¹⁶ or **EC**¹⁷.

Case Studies. PCDCNet was evaluated on major pollution events, including Spring Festival haze, severe Beijing pollution, and California wildfires, consistently providing early warnings and capturing pollution dynamics (Appendix A.8).

5 Conclusion

This work introduces PCDCNet, the Physical-Chemical Dynamics and Constraints Network, a scalable and interpretable surrogate model bridging deep learning efficiency with the physical consistency of numerical systems like CMAQ. By integrating emissions data, historical observations, and forecasted meteorology, PCDCNet captures complex spatiotemporal and nonlinear interactions through its LID, STD, and TAD modules, while Domain-Informed Constraints enforce alignment with atmospheric principles. Extensive experiments validate its state-of-the-art performance in PM_{2.5} and O₃ forecasting, demonstrating robust generalization and physical consistency. Future work will focus on optimizing scalability, refining chemical mechanisms, and expanding its application to larger or global regions, advancing air quality forecasting.

Acknowledgments

This work was supported by the National Natural Science Foundation of China (Grant No. 42450183, 12275020, 12135003, 12205025, 42461144209), the Ministry of Science and Technology of China (2023YFE0109000). Jingfang Fan is supported by the Fundamental Research Funds for the Central Universities. Shuo Wang acknowledges the financial support by China Scholarship Council (CSC) Grant No. 202106040117.

¹⁵<https://caiyunapp.com/map/>

¹⁶<https://www.ncei.noaa.gov/products/weather-climate-models/global-forecast>

¹⁷<https://www.ecmwf.int/>

References

- [1] Muhammad Naveed Anwar, Muneeba Shabbir, Eza Tahir, Mahnoor Iftikhar, Hira Saif, Ajwa Tahir, Malik Ashir Murtaza, Muhammad Fahim Khokhar, Mohammad Rehan, Mortaza Aghbashlo, et al. 2021. Emerging challenges of air pollution and particulate matter in China, India, and Pakistan and mitigating solutions. *Journal of Hazardous Materials* 416 (2021), 125851.
- [2] K Wyatt Appel, Sergey L Napelenok, Kristen M Foley, Haval OT Pye, Christian Hogrefe, Deborah J Lueken, Jesse O Bash, Shawn J Roselle, Jonathan E Pleim, Hosein Foroutan, et al. 2017. Description and evaluation of the Community Multiscale Air Quality (CMAQ) modeling system version 5.1. *Geoscientific model development* 10, 4 (2017), 1703–1732.
- [3] Kaifeng Bi, Lingxi Xie, Hengheng Zhang, Xin Chen, Xiaotao Gu, and Qi Tian. 2023. Accurate medium-range global weather forecasting with 3D neural networks. *Nature* 619, 7970 (2023), 533–538.
- [4] Cristian Bodnar, Wessel P Bruinsma, Ana Lucic, Megan Stanley, Johannes Brandstetter, Patrick Garvan, Maik Riechert, Jonathan Weyn, Haiyu Dong, Anna Vaughan, et al. 2024. Aurora: A foundation model of the atmosphere. *arXiv preprint arXiv:2405.13063* (2024).
- [5] Michael Brauer, Greg Freedman, Joseph Frostad, Aaron Van Donkelaar, Randall V Martin, Frank Dentener, Rita van Dingenen, Kara Estep, Heresh Amini, Joshua S Apte, et al. 2016. Ambient air pollution exposure estimation for the global burden of disease 2013. *Environmental science & technology* 50, 1 (2016), 79–88.
- [6] Marshall Burke, Marissa L Childs, Brandon de la Cuesta, Minghao Qiu, Jessica Li, Carlos F Gould, Sam Heft-Neal, and Michael Wara. 2023. The contribution of wildfire to PM_{2.5} trends in the USA. *Nature* 622, 7984 (2023), 761–766.
- [7] Baozhang Chen, Sheng Zhong, Nicholas AS Hamm, Hong Liao, Tong Zhu, Huifang Zhang, Lifeng Guo, Kun Hou, et al. 2024. Region-oriented simultaneously joint two-pollutant control strategies are required to substantially reduce deaths attributed to both PM_{2.5} and ozone pollution in China. *Atmospheric Environment* 334 (2024), 120708.
- [8] Han Chen, Weihang Zhang, and Lifang Sheng. 2025. Canadian record-breaking wildfires in 2023 and their impact on US air quality. *Atmospheric Environment* 342 (2025), 120941.
- [9] Ricky TQ Chen, Yulia Rubanova, Jesse Bettencourt, and David K Duvenaud. 2018. Neural ordinary differential equations. In *NeurIPS*.
- [10] Tianqi Chen and Carlos Guestrin. 2016. Xgboost: A scalable tree boosting system. In *ACM SIGKDD*. 785–794.
- [11] Ziyue Chen, Danlu Chen, Chuanfeng Zhao, Mei-po Kwan, Jun Cai, Yan Zhuang, Bo Zhao, Xiaoyan Wang, Bin Chen, Jing Yang, et al. 2020. Influence of meteorological conditions on PM_{2.5} concentrations across China: A review of methodology and mechanism. *Environment international* 139 (2020), 105558.
- [12] Ziyue Chen, Xiaoming Xie, Jun Cai, Danlu Chen, Bingbo Gao, Bin He, Nianliang Cheng, and Bing Xu. 2018. Understanding meteorological influences on PM_{2.5} concentrations across China: a temporal and spatial perspective. *Atmospheric Chemistry and Physics* 18, 8 (2018), 5343–5358.
- [13] Johanna Einsiedler, Yun Cheng, Franz Papst, and Olga Saukh. 2021. Interpretable and Transferable Models to Understand the Impact of Lockdown Measures on Local Air Quality. *arXiv preprint arXiv:2011.10144* (2021).
- [14] Christopher Emery, Kirk Baker, Gary Wilson, and Greg Yarwood. 2024. Comprehensive Air Quality Model with Extensions: Formulation and Evaluation for Ozone and Particulate Matter over the US. *Atmosphere* 15, 10 (2024).
- [15] Matthias Fey and Jan Eric Lenssen. 2019. Fast graph representation learning with PyTorch Geometric. In *ICLR Workshop*.
- [16] Chinese Society for Environmental Sciences. 2024. Technical guideline on city-level air pollutant emission inventory development. T/CSES 144–2024. <https://www.ttbz.org.cn/StandardManage/Detail/108461/>.
- [17] Zhaoqi Gao and Xuehua Zhou. 2024. A review of the CAMx, CMAQ, WRF-Chem and NAQPMS models: Application, evaluation and uncertainty factors. *Environmental Pollution* 343 (2024), 123183.
- [18] Guannan Geng, Yuxi Liu, Yang Liu, Shigan Liu, Jing Cheng, Liu Yan, Nana Wu, Hanwen Hu, Dan Tong, Bo Zheng, et al. 2024. Efficacy of China's clean air actions to tackle PM_{2.5} pollution between 2013 and 2020. *Nature Geoscience* (2024), 1–8.
- [19] Kethmi Hirushini Hettige, Jiahao Ji, Shili Xiang, Cheng Long, Gao Cong, and Jingyuan Wang. 2024. AirPhyNet: Harnessing Physics-Guided Neural Networks for Air Quality Prediction. In *ICLR*.
- [20] Peter V Hobbs. 2000. *Introduction to atmospheric chemistry*. Cambridge University Press.
- [21] Tangyan Hou, Shaocai Yu, Yaping Jiang, Xue Chen, Yibo Zhang, Mengying Li, Zhen Li, Zhe Song, Pengfei Li, Jianmin Chen, et al. 2022. Impacts of chemical initial conditions in the WRF-CMAQ model on the ozone forecasts in eastern China. *Aerosol and Air Quality Research* 22, 7 (2022), 210402.
- [22] Mark Z Jacobson. 1999. *Fundamentals of atmospheric modeling*. Cambridge university press.
- [23] Guolin Ke, Qi Meng, Thomas Finley, Taifeng Wang, Wei Chen, Weidong Ma, Qiwei Ye, and Tie-Yan Liu. 2017. Lightgbm: A highly efficient gradient boosting decision tree. In *NeurIPS*.
- [24] Thomas N Kipf and Max Welling. 2017. Semi-supervised classification with graph convolutional networks. In *ICLR*.
- [25] Remi Lam, Alvaro Sanchez-Gonzalez, Matthew Willson, Peter Wirmsberger, Meire Fortunato, Ferran Alet, Suman Ravuri, Timo Ewalds, Zach Eaton-Rosen, Weihua Hu, et al. 2023. Learning skillful medium-range global weather forecasting. *Science* 382, 6677 (2023), 1416–1421.
- [26] Jiali Li, Shaocai Yu, Xue Chen, Yibo Zhang, Mengying Li, Zhen Li, Zhe Song, Weiping Liu, Pengfei Li, Min Xie, et al. 2022. Evaluation of the WRF-CMAQ model performances on air quality in China with the impacts of the observation nudging on meteorology. *Aerosol and Air Quality Research* 22, 4 (2022), 220023.
- [27] Ke Li, Daniel J Jacob, Hong Liao, Jia Zhu, Viral Shah, Lu Shen, Kelvin H Bates, Qiang Zhang, and Shixian Zhai. 2019. A two-pollutant strategy for improving ozone and particulate air quality in China. *Nature Geoscience* 12, 11 (2019), 906–910.
- [28] Lianfa Li, Jinfeng Wang, Meredith Franklin, Qian Yin, Jiajie Wu, Gustau Camps-Valls, Zhiping Zhu, Chengyi Wang, Yong Ge, and Markus Reichstein. 2023. Improving air quality assessment using physics-inspired deep graph learning. *npj Climate and Atmospheric Science* 6, 1 (2023), 152.
- [29] Meng Li, Huan Liu, Guannan Geng, Chaopeng Hong, Fei Liu, Yu Song, Dan Tong, Bo Zheng, Hongyang Cui, Hanyang Man, et al. 2017. Anthropogenic emission inventories in China: a review. *National Science Review* 4, 6 (2017), 834–866.
- [30] Yasong Li, Tijian Wang, Mengmeng Li, Yawei Qu, Hao Wu, Min Xie, et al. 2024. Exploring the role of aerosol-ozone interactions on O₃ surge and PM_{2.5} decline during the clean air action period in Eastern China 2014–2020. *Atmospheric Research* 302 (2024), 107294.
- [31] Yong Liu, Tengge Hu, Haoran Zhang, Haixu Wu, Shiyu Wang, Lintao Ma, and Mingsheng Long. 2023. iTransformer: Inverted Transformers Are Effective for Time Series Forecasting. In *ICLR*.
- [32] Jing Lu, Yuhu Zhang, Mingxing Chen, Lu Wang, Shaohua Zhao, Xiao Pu, and Xuegang Chen. 2021. Estimation of monthly 1 km resolution PM_{2.5} concentrations using a random forest model over “2+26” cities, China. *Urban Climate* 35 (2021), 100734.
- [33] Xiao Lu, Lin Zhang, Xiaolin Wang, Meng Gao, Ke Li, Yuzhong Zhang, Xu Yue, and Yuanhang Zhang. 2020. Rapid increases in warm-season surface ozone and resulting health impact in China since 2013. *Environmental Science & Technology Letters* 7, 4 (2020), 240–247.
- [34] Soon-Young Park, Uzzal Kumar Dash, Jinhyeok Yu, Keiya Yumimoto, Itsushi Uno, and Chul Han Song. 2021. Implementation of an ensemble Kalman filter in the community multiscale air quality model (CMAQ model v5.1) for data assimilation of ground-level PM_{2.5}. *Geoscientific Model Development Discussions* 2021 (2021), 1–35.
- [35] Yanlin Qi, Qi Li, Hamed Karimian, and Di Liu. 2019. A hybrid model for spatiotemporal forecasting of PM_{2.5} based on graph convolutional neural network and long short-term memory. *Science of the Total Environment* 664 (2019), 1–10.
- [36] Yawei Qu, Tijian Wang, Cheng Yuan, Hao Wu, Libo Gao, Congwu Huang, Yasong Li, Mengmeng Li, and Min Xie. 2023. The underlying mechanisms of PM_{2.5} and O₃ synergistic pollution in East China: Photochemical and heterogeneous interactions. *Science of the Total Environment* 873 (2023), 162434.
- [37] S Trivikrama Rao, Huiying Luo, Marina Astitha, Christian Hogrefe, Valerie Garcia, and Rohit Mathur. 2020. On the limit to the accuracy of regional-scale air quality models. *Atmospheric chemistry and physics* 20, 16 (2020), 1627–1639.
- [38] John H Seinfeld and Spyros N Pandis. 2016. *Atmospheric chemistry and physics: from air pollution to climate change*. John Wiley & Sons.
- [39] Bhupal Shrestha, Jerald A Brotzge, and Junhong Wang. 2022. Observations and impacts of long-range transported wildfire smoke on air quality across New York state during July 2021. *Geophysical Research Letters* 49, 19 (2022), e2022GL100216.
- [40] Pierre Sicard, Paola Crippa, Alessandra De Marco, Stefano Castruccio, Paolo Giani, Juan Cuesta, Elena Paoletti, Zhaozhong Feng, and Alessandro Anav. 2021. High spatial resolution WRF-Chem model over Asia: Physics and chemistry evaluation. *Atmospheric Environment* 244 (2021), 118004.
- [41] Yongzhao Sun and Xiaoyan Wang. 2022. Meteorological factor contributions to the seesaw concentration pattern between PM_{2.5} and O₃ in Shanghai. *Frontiers in Environmental Science* 10 (2022), 1015723.
- [42] Chunyang Wang, Yanmin Zhu, Tianzi Zang, Haobing Liu, and Jiadi Yu. 2021. Modeling inter-station relationships with attentive temporal graph convolutional network for air quality prediction. In *ACM WSDM*. 616–634.
- [43] Pengfei Wang, Hao Guo, Jianlin Hu, Sri Harsha Kota, Qi Ying, and Hongliang Zhang. 2019. Responses of PM_{2.5} and O₃ concentrations to changes of meteorology and emissions in China. *Science of the Total Environment* 662 (2019), 297–306.
- [44] Shuo Wang, Yanran Li, Jiang Zhang, Qingye Meng, Lingwei Meng, and Fei Gao. 2020. PM_{2.5}-GNN: A domain knowledge enhanced graph neural network for pm_{2.5} forecasting. In *ACM SIGSPATIAL*. 163–166.
- [45] Yuxuan Wang, Haixu Wu, Jiaxiang Dong, Guo Qin, Haoran Zhang, Yong Liu, Yuzhong Qiu, Jianmin Wang, and Mingsheng Long. 2024. Timexer: Empowering transformers for time series forecasting with exogenous variables. In *NeurIPS*.
- [46] Qingyang Xiao, Guannan Geng, Tao Xue, Shigan Liu, Cilan Cai, Kebin He, and Qiang Zhang. 2021. Tracking PM_{2.5} and O₃ pollution and the related health

- burden in China 2013–2020. *Environmental science & technology* 56, 11 (2021), 6922–6932.
- [47] Hui Yang, Xinyuan Huang, Daniel M Westervelt, Larry Horowitz, and Wei Peng. 2023. Socio-demographic factors shaping the future global health burden from air pollution. *Nature Sustainability* 6, 1 (2023), 58–68.
- [48] Huanbi Yue, Chunyang He, Qingxu Huang, Dan Yin, and Brett A Bryan. 2020. Stronger policy required to substantially reduce deaths from PM_{2.5} pollution in China. *Nature Communications* 11, 1 (2020), 1462.
- [49] Biao Zhang and Rico Sennrich. 2019. Root mean square layer normalization. In *NeurIPS*.
- [50] Bo Zheng, Dan Tong, Meng Li, Fei Liu, Chaopeng Hong, Guannan Geng, Haiyan Li, Xin Li, Liqun Peng, Ji Qi, et al. 2018. Trends in China's anthropogenic emissions since 2010 as the consequence of clean air actions. *Atmospheric Chemistry and Physics* 18, 19 (2018), 14095–14111.

A Appendices

A.1 Related Work

A.1.1 Numerical Models for AQF. Numerical models like CMAQ [2], WRF-Chem [40], and CAMx [14] are widely used for AQF. They solve PDEs to simulate pollutant dynamics. Their interpretability and alignment with physical and chemical principles make them invaluable for understanding pollution transport and formation mechanisms. However, these models heavily rely on emission inventories, which are often uncertain, and their high computational cost renders them impractical for real-time applications. Furthermore, these models are not inherently designed to assimilate real-time observational data, limiting their ability to capture dynamic events like sudden pollution spikes [34], and reducing their effectiveness for timely forecasting. Despite these limitations, their robustness and interpretability offer valuable guidance for integrating domain knowledge into AI models.

A.1.2 Deep Learning Models for AQF. Deep learning has become a promising alternative, offering computational efficiency and the ability to model complex patterns in observational data. Methods such as Pangu-Weather [3] and GraphCast [25] leverage AI for meteorological forecasting but are not designed for AQF, often ignoring emissions and pollutant-specific dynamics. Within AQF, recurrent models (e.g., GRU, LSTM) capture temporal patterns, while graph-based methods (e.g., GC-LSTM [35], PM_{2.5}-GNN [44]) model spatial dependencies. AirPhyNet [19] incorporates physics-informed modeling using neural ordinary differential equations (neural ODEs) [9] to simulate pollutant dynamics like advection and diffusion. While this approach enhances interpretability and aligns predictions with physical principles, it is limited by the inherent constraints of neural ODEs, such as the inability to integrate additional meteorological variables effectively. This limitation reduces its flexibility and accuracy in capturing the multifaceted interactions of emissions, meteorology, and pollutants.

These models face challenges in handling varying pollution contexts. For instance, models trained on high-pollution regions often underperform in low-pollution scenarios due to their reliance on data-driven learning. Moreover, many deep learning approaches overlook emissions data or fail to incorporate domain knowledge, limiting their interpretability and accuracy in specialized AQF tasks.

A.1.3 Mixing Numerical Models & Deep Learning. The integration of numerical and deep learning models aims to combine their respective strengths. Numerical models provide interpretability and adherence to atmospheric principles but are computationally expensive. Deep learning methods, while efficient and capable of fitting observational data, often lack generalizability and domain-specific insights. Hybrid approaches, such as Aurora [4], attempt to bridge this gap but are limited by their dependence on structured reanalysis data, lack of emissions modeling, and absence of station-level observations.

PCDCNet addresses these challenges by combining emissions, meteorology, and physical-chemical constraints in a unified framework. It integrates the interpretability of numerical models with the efficiency of deep learning, enabling accurate and scalable AQF. By

explicitly modeling pollutant interactions and leveraging domain-informed constraints, PCDCNet provides a robust solution for real-time, station-level air quality forecasting.

A.2 Research Regions and Spatial Graph Construction

To ensure the effectiveness of spatial modeling in PCDCNet, we focus on two key regions in China: the Beijing-Tianjin-Hebei and Surrounding Areas (BTHSA) and the Yangtze River Delta (YRD). These regions are selected due to their distinct meteorological patterns, pollutant transport dynamics, and high-density air quality monitoring networks.

Figure 6 illustrates the constructed spatial graphs for these regions. Each orange node represents an air quality monitoring station, while blue edges denote spatial connections between nodes based on a geodesic distance threshold of 200 km. Major cities are highlighted in red, emphasizing their significant roles in regional pollutant transport and emissions.

The spatial graph captures critical dependencies for pollutant transport, including horizontal advection and diffusion, by linking nearby monitoring stations. These connections form the foundation for the graph-based components in PCDCNet, enabling effective spatiotemporal modeling. This graph-based structure ensures that both localized and regional pollutant dynamics are captured, aligning with real-world atmospheric processes.

A.3 Overview of Variables

The variables used in this study are categorized into three primary groups: **Air Pollutants**, **Meteorological Factors**, and **Emissions Data**. These variables capture key aspects of air quality dynamics, including pollutant concentrations, atmospheric conditions, and anthropogenic emissions, ensuring a robust input space for modeling.

A.3.1 Air Pollutants (X). Air pollutant variables represent the primary targets of the forecasting model, capturing concentrations of key pollutants:

- **PM_{2.5}** Fine particulate matter with a diameter of 2.5 micrometers or smaller ($\mu\text{g}/\text{m}^3$).
- **O₃** Ground-level O₃ ($\mu\text{g}/\text{m}^3$), a secondary pollutant influenced by precursor emissions and meteorological conditions.

A.3.2 Meteorological Factors (P). Meteorological variables describe the atmospheric conditions influencing pollutant dispersion, chemical reactions, and deposition:

- **t2m** 2-meter air temperature (K).
- **d2m** 2-meter dew point temperature (K).
- **tp** Total precipitation (m).
- **sp** Surface pressure (Pa).
- **blh** Boundary layer height (m), a key factor in vertical mixing.
- **msdswrf (swr)** Mean surface downward shortwave radiation flux (W/m^2), influencing photochemical reactions like O₃ formation.
- **u100, v100** Wind components at 100m altitude (m/s), critical for pollutant advection.

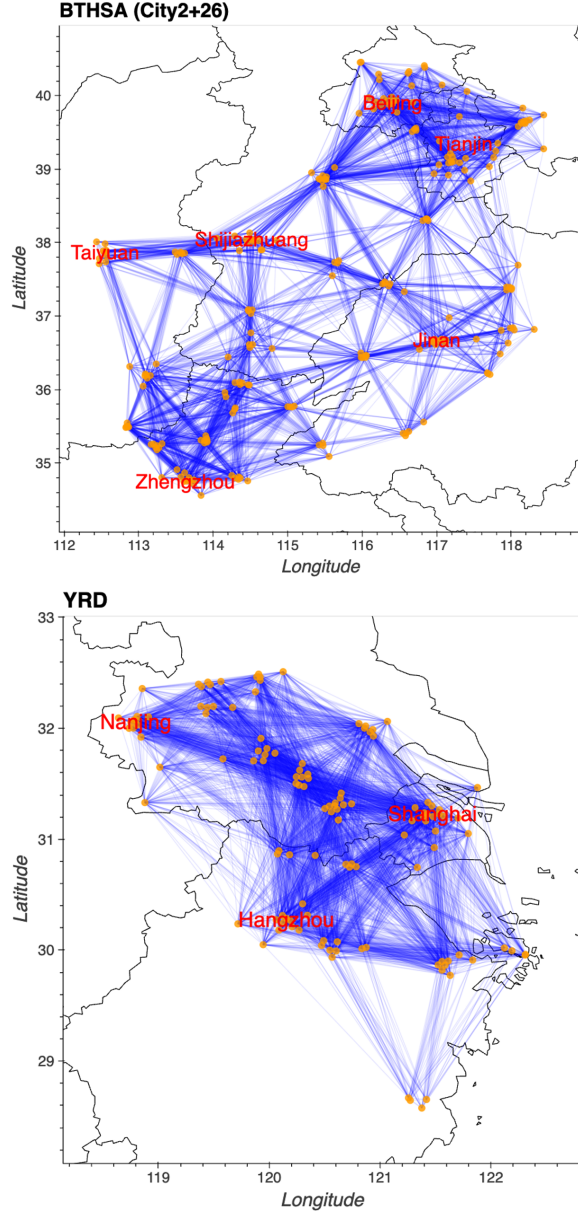


Figure 6: Research regions and constructed spatial graphs for the Beijing-Tianjin-Hebei and Surrounding Areas (BTHSA, top) and the Yangtze River Delta (YRD, bottom). Each orange node represents a monitoring station, and blue edges indicate spatial connections based on a 200 km geodesic distance threshold. Major cities are labeled in red, highlighting their central role in the regional graph structure. These graphs capture the spatial dependencies necessary for pollutant transport modeling and serve as the basis for graph-based components in our framework.

A.3.3 Emissions Data (Q). Emissions data quantify anthropogenic contributions to air quality and include:

- PM_{2.5} Fine particulate matter emissions (*ton*).
- PM₁₀ Coarse particulate matter emissions (*ton*).
- NO_x Nitrogen oxides (*ton*), precursors to O₃ and nitrate aerosol.
- VOC Volatile organic compounds (*ton*), precursors to O₃.
- NH₃ Ammonia (*ton*), contributing to secondary particulate formation.
- SO₂ Sulfur dioxide (*ton*), a precursor to sulfate aerosols.

A.3.4 Data Sources. The data were compiled from multiple authoritative sources, including:

- **Meteorology** ERA5 reanalysis data for high-resolution atmospheric parameters.
- **Emissions** MEIC (Multi-resolution Emission Inventory for China) for emissions statistics.
- **Air Pollutants** Observations from ground-based monitoring stations across China.

A.4 Notation Table

To aid in understanding the methodology and components of PCDCNet, Table 2 summarizes the key symbols and their corresponding descriptions used throughout the paper.

Table 2: Summary of Symbols Used in the Methodology

Symbol	Description
X^t, \hat{X}^t	Observed and predicted pollutant concentrations (e.g., PM _{2.5} , O ₃) at time t .
P^t, Q^t	Meteorological and emission variables (e.g., P_{t2m}^t for temperature, $Q_{NO_x}^t$ for NO _x emissions).
T', T	Historical window (T') and prediction window (T) lengths.
$\mathcal{G} = (\mathcal{V}, \mathcal{E})$	Station graph: \mathcal{V} (nodes), \mathcal{E} (edges).
$v, v', \mathcal{N}(v)$	A station node v , its neighboring node v' , and the set of all neighbors $\mathcal{N}(v)$.
\mathcal{F}_Θ	The model with learnable parameters Θ , integrating meteorology, emissions, and spatiotemporal dynamics.
H^t, E^t	Hidden states where H^t represents the rate of change in pollutant, meteorology, and emissions interactions, while E^t captures localized physical-chemical interactions.
M^t, \hat{X}_M^t	Aggregated message (M^t) for pollutant transport and its readout (\hat{X}_M^t) via STD module.
\mathcal{L}_{DIC}	Domain-Informed Constraint loss for enforcing physical consistency.
u, ∇, Δ	Wind vector (u), spatial gradient operator (∇) for pollutant advection and diffusion, and temporal difference operator (Δ) representing changes along the time dimension.
$d_{vv'}$	Geodesic distance between stations v and v' .

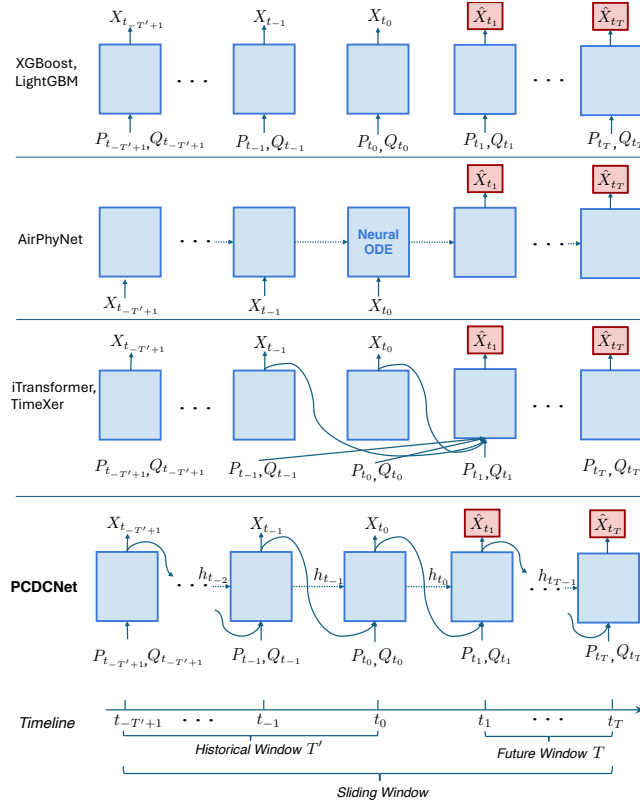


Figure 7: Comparison of input-output frameworks in air quality prediction. XGBoost and LightGBM process each time step independently. AirPhyNet links inputs sequentially via NeuralODEs [9]. Transformer-based models (e.g., iTransformer, TimeXer) capture dependencies across historical windows. PCDCNet integrates emissions, meteorology, and historical air quality using recurrent mechanisms and sliding windows, enabling spatiotemporal and physical-chemical dynamic modeling.

A.5 Input-Output Frameworks in Air Quality Prediction

Air quality forecasting (AQF) systems adopt diverse input-output frameworks tailored to their design goals. Figure 7 summarizes the paradigms of representative models:

- **XGBoost and LightGBM:** These models predict pollutant concentrations for each time step independently, leveraging historical meteorology and emissions but lacking temporal dependency modeling.
- **AirPhyNet:** Introduces sequential modeling using NeuralODEs [9], focusing on pollutant dynamics but limited by its inability to incorporate forecasted meteorology or emissions.
- **Transformer-based Models** (e.g., iTransformer, TimeXer): Utilize self-attention for capturing long-range temporal dependencies across historical windows. However, these models often exclude emissions and domain-specific constraints, limiting their interpretability.

- **PCDCNet:** A unified framework that incorporates historical and forecasted meteorology, emissions, and pollutant data via recurrent mechanisms and sliding windows. It explicitly integrates spatiotemporal dependencies and physical-chemical dynamics, ensuring accurate predictions.

This unified approach aligns with real-world AQF requirements, bridging the gap between computational efficiency and domain-specific modeling, a feature traditional numerical models lack.

A.6 Baseline Model Comparison

Table 3 presents a comparison of baseline models based on their core capabilities. The table highlights key features such as whether the model is specifically designed for air quality forecasting (AQF), supports temporal dependencies (Temp), handles multivariate predictions (MultiV), incorporates future exogenous variables (Exog), models spatial correlations (Spat), and integrates physical constraints (Phy).

Traditional methods like XGBoost and LightGBM lack temporal and spatial modeling capabilities, limiting their suitability for AQF tasks. Advanced models such as AirPhyNet and PM_{2.5}-GNN introduce spatial and temporal dynamics but fail to fully integrate exogenous variables or enforce physical constraints. On the other hand, PCDCNet and CMAQ comprehensively address all listed capabilities, providing robust solutions for accurate and interpretable air quality forecasting.

Table 3: Comparison of baseline models based on their native capabilities. Columns represent: AQF – whether the model is specifically designed for air quality forecasting; Temp – models temporal dependencies; MultiV – supports multivariate predictions; Exog – incorporates future exogenous variables; Spat – models spatial correlations; Phy – integrates physical constraints.

Methods	AQF	Temp	MultiV	Exog	Spat	Phy
XGBoost	✗	✗	✗	✓	✗	✗
LightGBM	✗	✗	✗	✓	✗	✗
GC-LSTM	✓	✓	✗	✗	✓	✗
PM _{2.5} -GNN	✓	✓	✗	✓	✓	✗
iTransformer	✗	✓	✓	✗	✗	✗
TimeXer	✗	✓	✓	✗	✗	✗
AirPhyNet	✓	✓	✗	✗	✓	✓
CMAQ	✓	✓	✓	✓	✓	✓
PCDCNet	✓	✓	✓	✓	✓	✓

A.7 Evaluation Metrics

To evaluate model performance, we use the following standard forecasting metrics:

Mean Absolute Error (MAE).

$$MAE = \frac{1}{N} \sum_{n=1}^N |\hat{X}_n - X_n|. \quad (17)$$

Root Mean Square Error (RMSE).

$$\text{RMSE} = \sqrt{\frac{1}{N} \sum_{n=1}^N (\hat{X}_n - X_n)^2}. \quad (18)$$

A.8 Detailed Deployment and Case Studies

A.8.1 Nationwide Air Quality During Festival. Figure 8 shows nationwide air quality distribution during the Chinese New Year and Spring Festival periods in 2025. The model successfully captured the severe pollution caused by extensive firework activities in regions like Changsha, predicting both the intensity of pollution and its eventual dissipation. This case highlights PCDCNet’s generalization capability to regions outside the training dataset and its ability to model short-term anthropogenic impacts.



Figure 8: Nationwide air quality during New Year’s Eve and Spring Festival, highlighting severe pollution in Changsha caused by fireworks and its eventual dissipation forecasting.

A.8.2 Extreme Pollution in Beijing. Figure 9 illustrates a pollution episode in Beijing on January 31, 2025. The system forecasted the event 72 hours in advance, capturing the rapid PM_{2.5} buildup due to high-pressure stagnation and local emissions. The prediction aligned closely with observed data, accurately signaling the event’s onset and dissipation. This early warning capability underscores PCDCNet’s utility in proactive air quality management.

A.8.3 California Wildfire Case. In January 2025, wildfires in California caused severe air quality deterioration across the Los Angeles region. Figure 10 visualizes the event progression, with PCDCNet capturing the pollutant spread driven by prevailing winds. The system’s accurate tracking of wildfire-induced pollution demonstrates its versatility in addressing diverse atmospheric scenarios [6]¹⁸.

A.8.4 System Scalability and Performance. To ensure robustness, the system was tested under high-demand conditions with concurrent API requests. Figure 11 showcases latency metrics, including P99, P95, and average latency, measured over a week. The results

¹⁸<https://www.who.int/health-topics/wildfires>

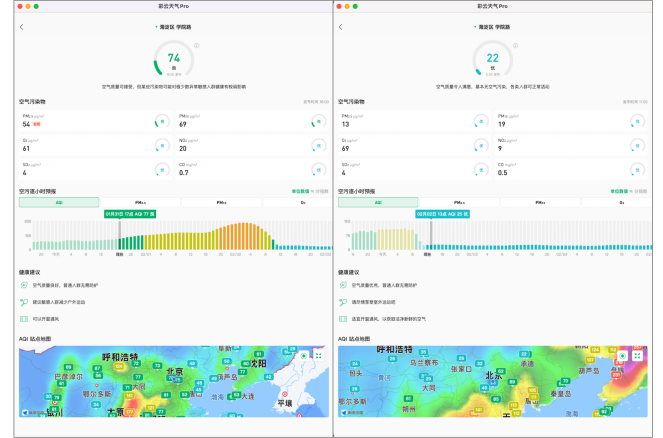


Figure 9: Model prediction (left) and real-world observation (right) for a pollution episode in Beijing, highlighting the system’s early warning capability.

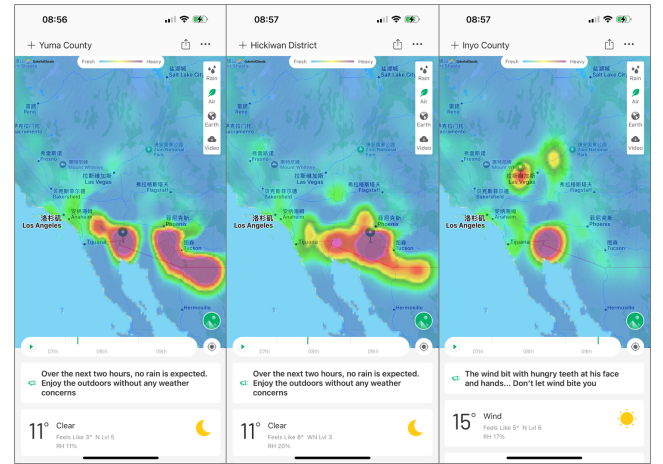


Figure 10: Air quality dynamics during California wildfires in January 2025, showcasing PCDCNet’s ability to track wildfire-induced pollution.

demonstrate the system’s ability to handle high query-per-second (QPS) loads without performance degradation, affirming its scalability for public deployment.

A.8.5 Cross-Platform Accessibility. PCDCNet’s deployment ensures easy access across multiple platforms. Users can download the **ColorfulClouds Weather** application from the Apple App Store or Android App Market for a comprehensive air quality forecasting experience. Alternatively, for those preferring a no-download option, the system is fully accessible through the web-based interface: <https://caiyunapp.com/map/>, offering real-time air quality predictions directly via any browser.

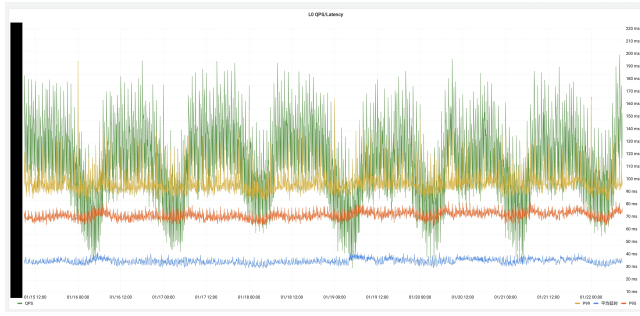


Figure 11: API performance metrics during deployment, showing low latency and consistent performance under high load conditions.



Figure 12: Real-time air quality visualization on the Caiyun web-based platform (Website: <https://caiyunapp.com/map>). The system provides 72-hour air quality forecasts, accessible without downloading an app, offering a seamless user experience directly via any browser.

A.9 Recognition in Competition

Excellence in Air Quality Forecasting Competition. The effectiveness of PCDCNet has been further validated through its performance in real-world competitive scenarios. PCDCNet achieved **first place in median performance** in the multi-city forecasting task of the prestigious “Air Quality Forecasting in the Guangdong-Hong Kong-Macao Region 2024” competition, hosted by the China National Environmental Monitoring Center (CNEMC)¹⁹.

This competition provided a rigorous benchmark for air quality forecasting models, requiring participants to produce accurate multi-day predictions across multiple cities in the Guangdong-Hong Kong-Macao region. PCDCNet’s robust performance, particularly in capturing multi-day forecast trends, highlighted its advanced

¹⁹National Ambient Air Quality Forecasting Model Comparison Platform: <http://124.128.14.106:10086/noticeDetail/66bef8dc65cfab60187f6887>

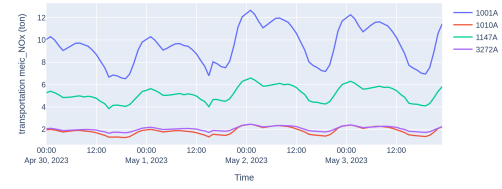


Figure 13: Temporal variation of NO_x emissions at four air quality monitoring stations: 1001A (Beijing city center), 1010A (Beijing suburban), 1147A (Shanghai city center), and 3272A (Shanghai suburban). The data, converted to UTC+0, highlights distinct morning and evening peaks due to traffic-related NO_x emissions. Urban stations exhibit higher levels compared to suburban stations.

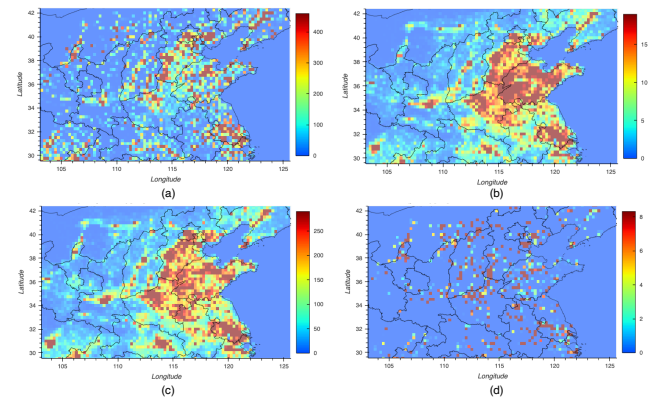


Figure 14: Spatial distribution of emissions over the study region: (a) NO_x emissions from the industrial sector (tons). (b) Transport-related PM_{2.5} emissions (tons). (c) Transport-related NO_x emissions (tons). (d) Power sector PM_{2.5} emissions (tons). The maps showcase the spatial variability of emissions across different sectors, with industrial emissions and transport emissions concentrated in urban and industrial hubs.

capabilities and domain-informed design, reinforcing its practical applicability and reliability in real-world forecasting tasks.

A.10 Emissions Data Analysis

The emissions data analyzed in this study include both temporal and spatial dimensions. The time series in Figure 13 demonstrates processed NO_x emissions from the transportation sector at key air quality stations in Beijing (1001A, 1010A) and Shanghai (1147A, 3272A). The temporal trends reveal distinct peaks during morning and evening rush hours, aligning with traffic patterns. Emissions levels are notably higher at urban stations (1001A and 1147A) compared to suburban ones (1010A and 3272A), underscoring the significant contribution of transportation to NO_x emissions in urban areas.

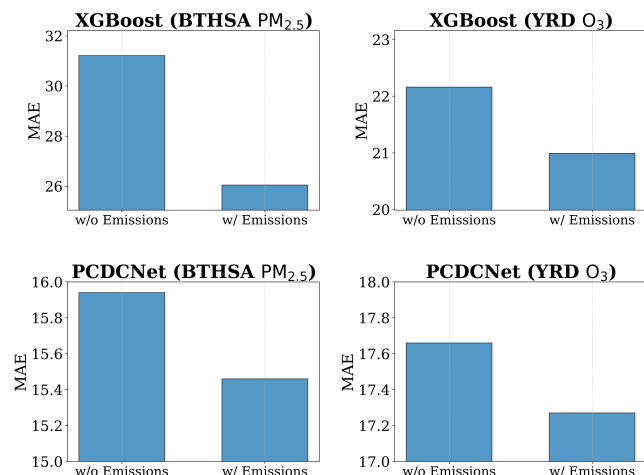


Figure 15: MAE comparison for BTHSA PM_{2.5} and YRD O₃ predictions using XGBoost and PCDCNet, with and without emissions data.

The spatial distribution of emissions (Figure 14) provides insights into the geographic variability across sectors. Industrial NO_x emissions (Figure 14a) are concentrated around major industrial zones. Transport-related PM_{2.5} and NO_x emissions (Figs. 14b and 14c) are predominantly urban, reflecting the density of transportation networks in cities. Power sector PM_{2.5} emissions (Figure 14d) are distributed near energy generation facilities, indicating their localized impact. These spatial distributions emphasize the critical role of emissions from different sectors in shaping air quality across the region.

Figure 15 illustrates the impact of emissions data on air quality predictions for BTHSA (PM_{2.5}) and YRD (O₃). The results demonstrate that incorporating emissions data significantly reduces MAE for both traditional models like XGBoost and advanced models like PCDCNet. This highlights the critical role of emissions data in capturing pollutant dynamics, particularly for chemically reactive pollutants like O₃. The consistent improvements across regions and models underscore the necessity of emissions data in accurate and robust air quality forecasting.

A.11 Real-time Monitoring of Air Quality Forecast Accuracy

The real-time monitoring dashboard in Figure 16 presented above evaluates the accuracy of our air quality forecasting model. It provides key performance metrics for PM_{2.5} predictions across different forecast horizons (e.g., 6 hours, 24 hours, and 72 hours) and various regions. The dashboard tracks metrics such as Mean Absolute Error (MAE), Normalized Mean Bias (NMB), and Normalized Mean Error (NME), which are essential for assessing the model's prediction accuracy. The bar charts on the right display the current air quality levels in Beijing, showing concentrations of pollutants like PM_{2.5}, PM₁₀, O₃, and SO₂. This monitoring system ensures that the forecasted air quality is continuously evaluated, providing

real-time insights into model performance and facilitating further optimization of the forecasting system.

Received 20 February 2007; revised 12 March 2009; accepted 5 June 2009

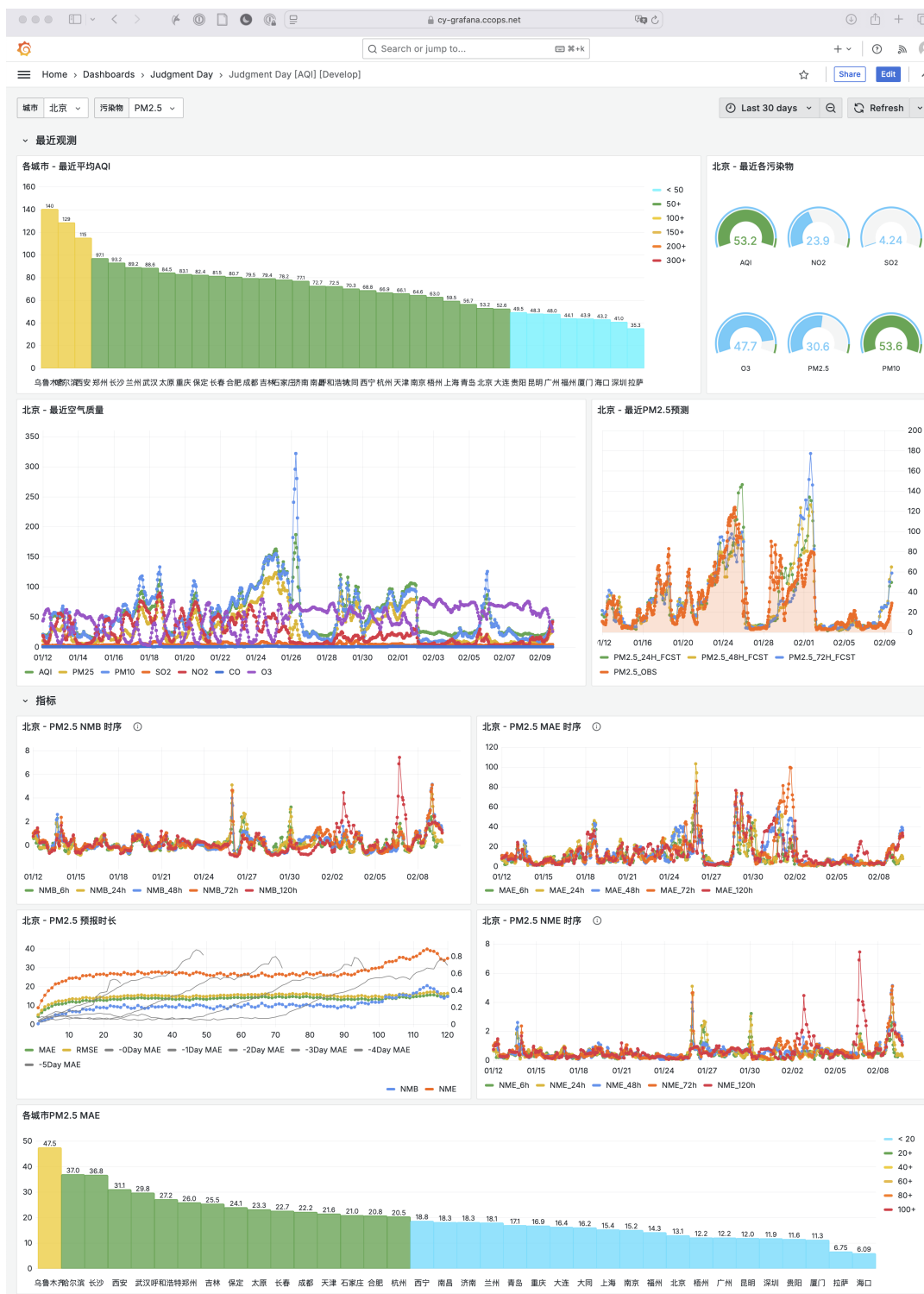


Figure 16: Online Real-Time Accuracy Monitoring of AQF